Effects of Particle-Phase Turbulence in Gas-Solid Flows

Christine M. Hrenya and Jennifer L. Sinclair
Dept. of Chemical Engineering, Carnegie Mellon University, Pittsburgh, PA 15213

Numerous experimental investigations on the vertical transport of dense gas–solid suspensions indicate that particles tend to segregate toward the tube wall. Although models based on the kinetic theory analogy can predict such patterns for perfectly elastic particle-particle collisions, the predictive ability of these models breaks down for inelastic collisions. In the present effort, a mathematical model is developed that incorporates two mechanisms that give rise to the lateral segregation of solids: interactions associated with individual particles based on a kinetic theory treatment and interactions associated with collections of particles based on an analogy with single-phase turbulent flows. Although these two mechanisms have been treated independently by previous workers, their combined contributions to the overall flow behavior have not been thoroughly investigated. The effect of such a treatment on the sensitivity of the model predictions to the inelasticity of particle–particle collisions is explored. A key element in eliminating the undue sensitivity appears to be a consideration of the effects associated with the collective motion of particles on the kinetic theory expressions. The resulting model can predict the expected segregation patterns for systems characterized by inelastic collisions, as well as many of the other salient features of vertical gas–solid flows.

Introduction

Particle-laden gaseous flows are used extensively in the chemical-process industries. An important class of applications that utilize such flows is reactions that involve both a gas phase and a solid-particulate phase. Examples include fluid catalytic cracking (FCC), coal combustion, and the production of high-purity alumina. For such reactions, circulating fluidized beds (CFBs) are often employed due to the advantages that they offer over the traditional bubbling fluidized beds: higher throughput, greater gas–solid contacting, and the allowance for continuous regeneration of catalyst. At present, however, these advantages are not being fully exploited due to the difficulties in predicting the complex hydrodynamics of gas–solid flows. For example, the general tendency of particles to segregate toward the pipe wall in the upward, vertical flow of a relatively dense gas–solid mixture has been well documented (e.g., Yerushalmi et al., 1978; Weinstein et al., 1984; Bader et al., 1988; Miller and Gidaspow, 1992). In the vertical riser reactor section of a CFB, the amount of such segregation will greatly affect the solids recirculation rate, the reaction rate, as well as the heat transfer rate. The physical mechanism responsible for the observed solids concentration patterns, however, is still not well understood, and such an understanding is crucial for the design of systems utilizing dispersed gas–solid flows.

The modeling work of Sinclair and Jackson (1989) demonstrated that the interaction between individual particles is capable of giving rise to the lateral segregation of solids observed in vertical tubes. More specifically, they described solid-phase stresses by making an analogy between the random particle motion arising from particle collisions and the thermal motion of molecules in a gas. Similar to gas-phase stresses, the pressure and viscosity of the solid phase depend on the intensity of the particle velocity fluctuations. Accordingly, the kinetic energy associated with the random particle motion is characterized by a "pseudothermal" or granular temperature, which is proportional to the mean square of the random component of particle velocity. Unlike true thermal energy, however, this pseudothermal or granular energy is

Correspondence concerning this article should be addressed to J. L. Sinclair.
Present addresses of: J. L. Sinclair, Dept. of Chemical and Environmental Engineering, University of Arizona, Tucson, AZ 85721; C. M. Hrenya, Honeywell Technology Center, 3660 Technology Drive, Minneapolis, MN 55418.

dissipated by inelastic particle–particle and particle–wall collisions. Thus, the solution of a separate equation representing the balance of pseudothermal energy is required in addition to the continuity and momentum balances for each phase. When applied to fully developed flow in a vertical pipe, the model equations indicate that the solids concentration is inversely proportional to the pseudothermal temperature. As a result, the model is able to predict a nonuniform concentration of solids.

Although this treatment was also able to predict much of the other complex flow behavior associated with vertical gas–solid systems (e.g., particle recirculation in systems with a net upflow of solids, existence of a flooding envelope), Pita and Sundaresan (1991) showed that the model exhibits an unrealistic degree of sensitivity to the coefficient of restitution, e. This coefficient of restitution is a measure of the inelasticity of particle–particle collisions; its value ranges from zero for perfectly inelastic collisions to unity for perfectly elastic collisions. To illustrate this undue sensitivity to e, Figures 1a and 1b show the radial profiles of solids volume fraction and pseudothermal temperature, respectively, obtained using the Sinclair and Jackson (1989) model for the conditions in Table 1. Model predictions are given for $e = 1.0$ and $e = 0.99$. For both cases, the particle–wall coefficient of restitution, e_w, is 0.9. For $e = 1.0$ and $e_w = 0.9$, the pseudothermal temperature is lowest at the pipe wall due to the inelastic particle–wall collisions. Correspondingly, the model predicts a relatively high concentration of particles near the wall. For $e = 0.99$ and $e_w = 0.9$, however, the segregation of particles appears at the core of the pipe due to the large drop in pseudothermal temperature caused by inelastic particle–particle collisions. Such unrealistic behavior was also observed by Ocone et al. (1993), who extended the model of Sinclair and Jackson (1989) to account for frictional forces transmitted between particles at points of sustained contact. Evidently, not all of the mechanical interactions present in the physical system are being included in these models.

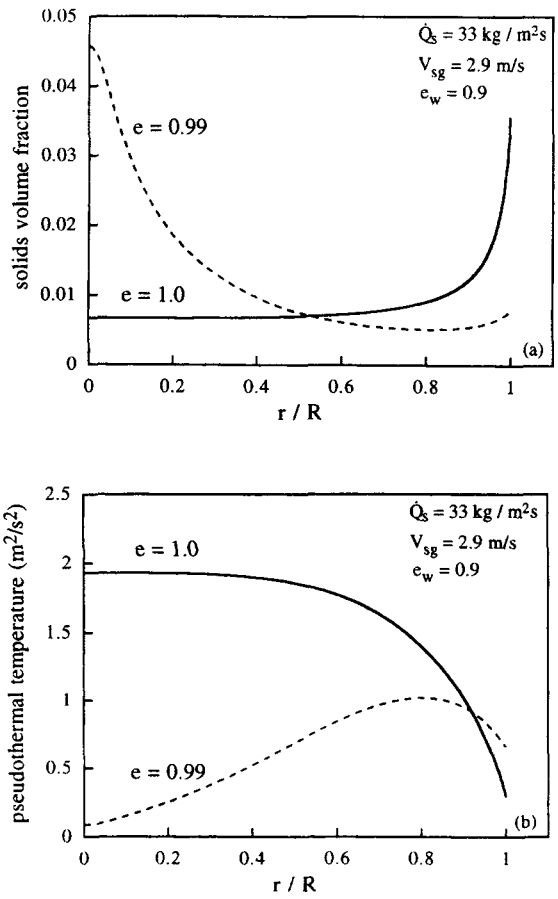

Figure 1. Sinclair and Jackson (1989) model: radial variation of (a) solids volume fraction and (b) pseudothermal temperature for conditions in Table 1.

Table 1. System Parameters Corresponding to Figures 1, 3 and 4

Pipe diameter (D)	7.5 cm
Particle diameter (d_p)	75 μm
Particle density (ρ_s)	1,654 kg/m^3
Gas density (ρ_g)	1.2 kg/m^3
Gas viscosity (μ_g)	1.81×10^{-5} kg/m·s
Solids volume fraction at closest packing (ϕ_{so})	0.65

One flow feature that is not accounted for in the preceding models is the presence of gas-phase turbulence. The importance of describing the effects of turbulent fluctuations in the gas phase, however, is quite different for dilute- and dense-phase flows. This difference becomes apparent when considering the relative magnitude of the terms present in the gas–phase momentum balance for fully developed, vertical gas-solid flows: diffusion (which includes both laminar and turbulent stresses), pressure drop, and drag force. In dilute-phase flows, the drag force is much smaller than the other forces due to the low concentration of solids. Thus, the description of turbulence as represented in the diffusion term is extremely important. Louge et al. (1991), Bolio et al. (1995), and Bolio and Sinclair (1995) incorporated the effects of gas-phase turbulence into their models by modifying single-phase turbulence closures to account for the presence of a dilute particle phase. These models were able to predict the significant flow features that have been observed experimentally in dilute gas–solid flows. In addition, these models were not found to be overly sensitive to the coefficient of restitution. However, unlike dilute-phase flows, flows in the dense-phase regime experience a significant drag force due to the high concentration of solids. As a result, the dominant forces in the gas-phase momentum balance are the pressure drop and the drag force, while the contribution of diffusion becomes negligible in comparison (Pita and Sundaresan, 1991 and 1993). The description of gas-phase turbulence is therefore relatively insignificant for dense-phase flows.

Another phenomenon that is associated with dense gas–solid flows and is not accounted for in the models previously described is the tendency of the *solid phase* to exhibit a "turbulent-like" behavior. For example, in the vertical gas–solid flow experiments of Yerushalmi et al. (1978) and Plumpe et al. (1993), large transient fluctuations in the suspension density were observed. These fluctuations give rise to time-dependent "Reynolds-like" stresses in the solid phase, as were in the annular shear-cell experiments of Savage and Sayed (1984). Similar behavior has also been noted in com-

puter simulations of granular flows, though it is important to distinguish between the two types of spatial inhomogeneities that have been described in the literature. The first type, which will be referred to as "particle-layering," was observed by Campbell and Brennen (1985) and Savage (1991). This microstructure forms near the solids packing limit and is characterized by the tendency of particles to align into layers in the direction of mean flow such that a fluid behavior can be maintained. With a slight increase in solids concentration, these systems will exhibit a solid behavior. The other type of microstructure, "particle packets," has been detected in the simulations performed by Hopkins and Louge (1991) and Walton et al. (1991). In these flows, collections of particles travel randomly about the pipe and continuously form and dissolve, similar to the motion of eddies in a single-phase turbulent fluid. In addition, these particle packets are found to be most prevalent at moderate solids concentration. Since the focus of this work is to describe gas–solid flows that are in the dense-phase regime but that are not close to the packed-bed limit, a consideration of the effects of the particle-layering microstructure is unnecessary. A description of the effects associated with the particle packets, however, is essential.

It is important to note that the kinetic theory expressions employed by the models described earlier do not account for the formation of any large spatial or temporal inhomogeneities. These expressions are obtained assuming molecular chaos, and thus are only applicable to systems in which the flow-field properties vary smoothly in space and time.

The effects associated with the collective motion of particle packets in dense gas–solid flows were first considered by Dasgupta et al. (1994). In their model, the fluctuations associated with collections of particles are described using an approach similar to that of single-phase turbulence. Namely, the governing equations are time-averaged, giving rise to several turbulence correlations that require modeling. However, the effects of "particle-phase turbulence" on the kinetic theory closures are neglected (i.e., these expressions are not time-averaged). Hence, the modeling of complex turbulence correlations is unnecessary.

Before discussing the details of the Dasgupta et al. (1994) model, it is helpful to examine the implications that this time-averaging treatment has on the particle segregation patterns of a fully developed vertical pipe flow. Based on the analogy between single-phase turbulence and particle-phase turbulence, two regimes of gas–solid flows can be identified: the "laminar" regime and the "turbulent" regime, both of which are depicted in Figure 2. In the laminar regime, only the random motion of individual particles is considered. In the turbulent regime, however, only the random motion of collections of particles is considered. The magnitude of the random velocity associated with collections of particles is defined by the turbulent kinetic energy of the particle phase, k_s, just as the magnitude of the random velocity associated with individual particles is defined by the pseudothermal temperature, T. Based on the limiting form of the time-averaged solids momentum balance, it is found that the solids volume fraction is inversely proportional to T in the laminar regime, as is the case for the model of Sinclair and Jackson (1989). Similarly, in the turbulent regime, the solids volume fraction is inversely proportional to k_s. Thus, two mechanisms exist that are responsible for particle segregation. As mentioned earlier, when only the laminar mechanism is considered, a segregation of particles is observed at the pipe center for $e < 1.0$ due to the large dissipation of pseudothermal energy. However, if the turbulent mechanism alone is considered, the solids concentration will always be highest at the wall since k_s, similar to the turbulent kinetic energy of single-phase flows, reaches a minimum at the wall. A complete model for dense-phase flows, though, must account for *varying* fluctuations both at the level of the individual particle and at the level of collections of particles. Thus, the resulting segregation patterns will depend on which of the two mechanisms dominate.

Although the Dasgupta et al. (1994) model does account for fluctuations of flow-field properties at both the level of the individual particle and the level of collections of particles, the pseudothermal temperature is assumed to be *constant*. Thus, if a constant value of T is chosen such that the laminar mechanism dominates, a uniform distribution of solids will be predicted across the tube radius. However, the constant value of the pseudothermal temperature arbitrarily chosen by Dasgupta et al. (1994) is such that the turbulent mechanism always dominates. As a result, the model always predicts a segregation of particles at the pipe wall. Furthermore, since a balance of pseudothermal energy is not solved, the value of the coefficient of restitution is no longer an input to the model. Hence, the model results are no longer a function of the inelasticity of particle–particle collisions.

The aim of the current work is to extend the dense, gas–solid flow model proposed by Dasgupta et al. (1994) to account for *variations* in fluctuations associated with both individual particles and collections of particles. Although the model is applicable to general flow conditions, attention here will be restricted to steady, fully developed flow in a vertical pipe. Initially, a model is presented in which the effects of particle-phase turbulence on the governing equations alone is considered (Model 1). It is shown that such a model cannot adequately describe the behavior of vertical gas–solid flows. However, by also accounting for the effects of particle-phase turbulence on the kinetic theory expressions, the resulting model (Model 2) is able to predict particle segregation at the wall without an undue sensitivity to inelastic particle–particle collisions, as well as many of the other salient features associated with such flows.

Model Development

Model 1: effects of particle-phase turbulence on the governing equations

The governing equations for the isothermal, incompressible flow of a fluid–solid mixture were developed using a continuum approach that replaces the point mechanical variables, such as velocities and pressures, with their corresponding local mean variables (Anderson and Jackson, 1967). Specifically, these equations are obtained by volume-averaging both the Navier–Stokes equations and the equations of motion of a single solid particle over a region in which the characteristic length scale is considerably larger than the interparticle distance and considerably smaller than the system dimensions. The resulting set of governing equations is given as:

$$\phi_g + \phi_s = 1 \tag{1}$$

$$\frac{\partial \phi_g}{\partial t} + \frac{\partial}{\partial x_i}(\phi_g V_{gi}) = 0 \tag{2}$$

$$\frac{\partial \phi_s}{\partial t} + \frac{\partial}{\partial x_i}(\phi_s V_{si}) = 0 \tag{3}$$

$$\rho_g \left[\frac{\partial V_{gi}}{\partial t} + V_{gj} \frac{\partial V_{gi}}{\partial x_j} \right] = -\frac{\partial P}{\partial x_i} - \frac{\partial \tau_{ij}}{\partial x_j} - \beta (V_{gi} - V_{si}) \tag{4}$$

$$\rho_s \left[\frac{\partial}{\partial t}(\phi_s V_{si}) + \frac{\partial}{\partial x_j}(\phi_s V_{si} V_{sj}) \right] = -\frac{\partial \sigma_{ij}}{\partial x_j} + \rho_s \phi_s g_i + \beta (V_{gi} - V_{si}), \tag{5}$$

where the subscripts g and s refer to the gas and solid phase, respectively; ϕ is the volume fraction; V_i is the velocity; ρ is the density; P is the gas-phase pressure; g_i is the gravity; β is the drag coefficient; and τ_{ij} and σ_{ij} are the stress tensors, defined in the compressive sense, associated with the gas and solid phases, respectively. Equations 1–3 represent the global, gas-phase, and solid-phase continuity balance, respectively, while Eqs. 4 and 5 represent a balance of gas-phase and solid-phase momentum, respectively. It should also be noted that the terms representing the gas-phase gravitational force and the reaction force on particles to pressure gradients associated with gas-phase accelerations have not been included in Eqs. 4 and 5 and are assumed negligible due to the low density of the gas phase.

In order to make the preceding set of equations explicit, expressions for the drag coefficient and the stress tensors are required. Because it is assumed that the length scales associated with particle-phase turbulence are much greater than the length scale established by volume-averaging, these expressions should describe the physical consequences associated with the "laminar" phenomena only. Accordingly, solid-phase stresses are described using the kinetic-theory analogy, thereby requiring the solution of an additional equation, the pseudothermal energy balance:

$$\frac{3}{2} \rho_s \left[\frac{\partial}{\partial t}(\phi_s T) + \frac{\partial}{\partial x_i}(\phi_s V_{si} T) \right] = -\frac{\partial q_i}{\partial x_i} - \sigma_{ij} \frac{\partial V_{si}}{\partial x_j} - \gamma, \tag{6}$$

where q_i represents the flux of pseudothermal energy, and γ represents the dissipation of pseudothermal energy due to inelastic particle–particle collisions.

Based on the approach used to describe single-phase turbulent flows, the presence of particle-phase turbulence in two-phase flows will be accounted for by the time-averaging of Eqs. 1–6 and the modeling of the resulting turbulence correlations. This time-averaging of the volume-averaged equations is only valid if the phenomena associated with the different scales of averaging are distinct and well-separated. In other words, the smallest length and time scale associated with particle-phase turbulence must be significantly larger than the length and time scale associated with the volume-averaging process. For the systems examined in this study, a significant separation of scales was shown to exist. The details of this analysis are given by Hrenya (1996).

The time-averaged form of the governing equations is obtained by applying Reynolds decomposition to each of the variables and then time-averaging the resulting equations. According to Reynolds decomposition, each variable is separated into a mean and fluctuating component. For example,

$$V_{gi} = \overline{V_{gi}} + V'_{gi}, \tag{7}$$

where an overbar denotes a time-averaged quantity and a prime denotes a fluctuating quantity. It is important to emphasize that Model 1 does not account for effects of particle-phase turbulence on the kinetic theory expressions (σ_{ij}, q_i, and γ). Instead, these terms are simply evaluated using the time-averaged variables:

$$\sigma_{ij} \approx \sigma_{ij}\left(\overline{\phi_s}, \overline{T}, \overline{V_{si}}, \overline{V_{sj}}\right); \qquad q_i \approx q_i(\overline{\phi_s}, \overline{T}); \qquad \gamma \approx \gamma(\overline{\phi_s}, \overline{T}). \tag{8}$$

Although this assumption is clearly an oversimplification, the reason for such a treatment is twofold. First, the turbulence correlations arising from the time-averaging of the kinetic theory expressions are extremely complex, making the modeling of such terms highly speculative. Perhaps more importantly, though, this treatment allows one to determine if accounting for the effects of particle-phase turbulence on the governing equations alone is capable of removing the extreme sensitivity to inelastic particle–particle collisions displayed by models that do not include any descriptions of particle-phase turbulence. With this in mind, the resulting time-averaged forms of Eqs. 1–6 are

$$\overline{\phi_g} + \overline{\phi_s} = 1 \tag{9}$$

$$\frac{\partial \overline{\phi_g}}{\partial t} + \frac{\partial}{\partial x_i}\left(\overline{\phi_g}\,\overline{V_{gi}} + \overline{\phi'_g V'_{gi}}\right) = 0 \tag{10}$$
(i)

$$\frac{\partial \overline{\phi_s}}{\partial t} + \frac{\partial}{\partial x_i}\left(\overline{\phi_s}\,\overline{V_{si}} + \overline{\phi'_s V'_{si}}\right) = 0 \tag{11}$$
(ii)

$$\rho_g \left[\frac{\partial \overline{V_{gi}}}{\partial t} + \overline{V_{gj}} \frac{\partial \overline{V_{gi}}}{\partial x_j} \right] = -\frac{\partial \overline{P}}{\partial x_i} - \frac{\partial \overline{\tau_{ij}}}{\partial x_j} - \rho_g \frac{\partial}{\partial x_j}\left(\overline{V'_{gi} V'_{gj}}\right) - \overline{\beta(V_{gi} - V_{si})} + \rho_g \left(\overline{V'_{gi} \frac{\partial V'_{gj}}{\partial x_j}} \right) \tag{12}$$
(iii)

$$\rho_s\left[\underbrace{\frac{\partial}{\partial t}\left(\overline{\phi_s}\,\overline{V_{si}}+\overline{\phi_s' V_{si}'}\right)}_{\text{(iv)}}+\frac{\partial}{\partial x_j}\left(\overline{\phi_s V_{si} V_{sj}}\right)\right]$$

$$=-\frac{\partial}{\partial x_j}\underbrace{\left[\sigma_{ij}\left(\overline{\phi_s},\overline{T},\overline{V_{si}},\overline{V_{sj}}\right)+\rho_s\overline{\phi_s V_{si}' V_{sj}'}\right]}_{\text{(v)}}$$

$$+\rho_s\overline{\phi_s}g_i+\overline{\beta(V_{gi}-V_{si})}-\rho_s\frac{\partial}{\partial x_j}\underbrace{\left[\overline{\phi_s' V_{sj}'}\,\overline{V_{si}}\right.}_{\text{(vi)}}$$

$$\left.\underbrace{+\overline{\phi_s' V_{si}'}\,\overline{V_{sj}}}_{\text{(vii)}}+\overline{\phi_s' V_{si}' V_{sj}'}\right] \quad (13)$$

$$\frac{3}{2}\rho_s\left[\underbrace{\frac{\partial}{\partial t}\left(\overline{\phi_s}\,\overline{T}+\overline{\phi_s' T'}\right)}_{\text{(viii)}}+\frac{\partial}{\partial x_i}\left(\overline{\phi_s V_{si}}\,\overline{T}\right)\right]$$

$$=-\frac{\partial}{\partial x_i}\underbrace{\left[q_i\left(\overline{\phi_s},\overline{T}\right)+\frac{3}{2}\rho_s\overline{\phi_s V_{si}' T'}\right]}_{\text{(ix)}}$$

$$-\overline{\sigma_{ij}}\left(\overline{\phi_s},\overline{T},\overline{V_{si}},\overline{V_{sj}}\right)\frac{\partial\overline{V_{si}}}{\partial x_j}-\gamma\left(\overline{\phi_s},\overline{T}\right)$$

$$-\frac{3}{2}\rho_s\frac{\partial}{\partial x_i}\underbrace{\left(\overline{T}\,\overline{V_{si}'\phi_s'}\right.}_{\text{(x)}}+\underbrace{\overline{V_{si}}\,\overline{\phi_s' T'}}_{\text{(xi)}}\underbrace{\left.\right)}+\underbrace{\rho_s\,\overline{\phi_s}\,\epsilon_s}_{\text{(xii)}}, \quad (14)$$

where ϵ_s represents the dissipation rate of the turbulent kinetic energy associated with particle packets. The final term in the pseudothermal energy balance (Eq. 14) does not appear rigorously from the time-averaging process, but is added to this equation based on the analogy with single-phase turbulent flows. In the same manner that turbulent kinetic energy of a single-phase fluid dissipates into true thermal heat, it is assumed that solid-phase turbulent kinetic energy will dissipate into pseudothermal heat. Thus, the dissipation rate of the particle-phase turbulent kinetic energy appears as a source term in the pseudothermal energy balance.

At this point, several simplifying assumptions are applied to the governing equations. As discussed earlier, the contribution of gas-phase diffusion is relatively unimportant in dense gas-solid flows. Thus, the second and third terms on the righthand side of Eq. 12, which represent laminar and turbulent diffusion of the gas phase, respectively, are ignored. In addition, third-order turbulence correlations are neglected, thereby eliminating the need to model the final term in Eq. 13. The final simplification deals with the time-averaged drag-force term, which appears in both Eqs. 12 and 13. In order to evaluate this term, the drag coefficient proposed by Wen and Yu (1965) is used:

$$\beta=\frac{3}{4}\frac{\rho_g}{d_p}\frac{(1-\phi_g)}{\phi_g^{2.7}}C_d\sqrt{(V_{gj}-V_{sj})^2}, \quad (15)$$

where

$$C_d=\frac{24}{\phi_g\,Re_p}\left[1+0.15(\phi_g\,Re_p)^{0.687}\right] \quad (16)$$

and

$$Re_p=\frac{\rho_g\,d_p\sqrt{(V_{gj}-V_{sj})^2}}{\mu_g}. \quad (17)$$

In the preceding expressions, d_p is the particle diameter, and μ_g is the intrinsic gas viscosity. However, since the expression for β is a nonlinear function of the gas-volume fraction and the velocities of both phases, it is approximated using a linearized form:

$$\beta\approx\beta\left(\overline{\phi_g},\overline{V_{gj}},\overline{V_{sj}}\right)+\left(\frac{\partial\beta}{\partial V_{gj}}\right)_{\overline{\phi_g},\overline{V_{gj}},\overline{V_{sj}}}V_{gj}'$$

$$+\left(\frac{\partial\beta}{\partial V_{sj}}\right)_{\overline{\phi_g},\overline{V_{gj}},\overline{V_{sj}}}V_{sj}'+\left(\frac{\partial\beta}{\partial\phi_g}\right)_{\overline{\phi_g},\overline{V_{gj}},\overline{V_{sj}}}\phi_g'. \quad (18)$$

Based on this approximation, the time-averaged drag force becomes

$$\overline{\beta(V_{gi}-V_{si})}=\beta\left(\overline{\phi_g},\overline{V_{gj}},\overline{V_{sj}}\right)\left(\overline{V_{gi}}-\overline{V_{si}}\right)$$

$$+\left(\frac{\partial\beta}{\partial V_{gj}}\right)_{\overline{\phi_g},\overline{V_{gj}},\overline{V_{sj}}}\left(\overline{V_{gj}'\,V_{gi}'}-\overline{V_{gj}'\,V_{si}'}\right)$$

$$+\left(\frac{\partial\beta}{\partial V_{sj}}\right)_{\overline{\phi_g},\overline{V_{gj}},\overline{V_{sj}}}\left(\overline{V_{sj}'\,V_{gi}'}-\overline{V_{sj}'\,V_{si}'}\right)$$

$$+\left(\frac{\partial\beta}{\partial\phi_g}\right)_{\overline{\phi_g},\overline{V_{gj}},\overline{V_{sj}}}\left(\overline{\phi_g'\,V_{gi}'}-\overline{\phi_g'\,V_{si}'}\right). \quad (19)$$

A further simplification of the preceding expression is possible if, as discussed by Dasgupta et al. (1994), attention is restricted to systems composed of "small" particles. As shown in Eq. 15, small particles give rise to large drag coefficients. If the drag coefficient is large enough, the slip velocity between phases is small in magnitude compared with each of the gas- and solid-phase fluctuating velocity components. As a result, $V_{gi}'\approx V_{si}'$ and Eq. 19 reduces to

$$\overline{\beta(V_{gi}-V_{si})}=\beta\left(\overline{\phi_g},\overline{V_{gj}},\overline{V_{sj}}\right)\left(\overline{V_{gi}}-\overline{V_{si}}\right). \quad (20)$$

It should be noted that this relation is valid only if the relaxation time of the gas velocity to conform to the solids velocity is significantly smaller than the smallest time scale associated with particle-phase turbulence. Again, this condition was found to be valid for the systems examined in this work (Hrenya, 1996).

With these simplifications, the turbulence correlations present in Eqs. 10–14 that require modeling are labeled (i)–(xii). Term (v) represents the "Reynolds stress" of the particle phase. Based on the analogy between single-phase turbulence and particle-phase turbulence, this correlation is described according to an eddy viscosity assumption:

$$\overline{V_{si}'\,V_{sj}'}=-\nu_{ts}\left(\frac{\partial\overline{V_{si}}}{\partial x_j}+\frac{\partial\overline{V_{sj}}}{\partial x_i}\right)+\frac{2}{3}\delta_{ij}\left(k_s+\nu_{ts}\frac{\partial\overline{V_{sk}}}{\partial x_k}\right), \quad (21)$$

where ν_{ts} is the eddy viscosity. The final term in the preceding expression, which does not appear for single-phase turbulent flows, is required in order to satisfy the definition of the turbulent kinetic energy of the solid phase:

$$k_s = \frac{1}{2}(\overline{V'_{si}\ V'_{si}}). \tag{22}$$

Furthermore, isotropy of the fluctuating velocity components is assumed such that:

$$\frac{2}{3}k_s = \overline{V'_{sr}\ V'_{sr}} = \overline{V'_{sz}\ V_{sz}} = \overline{V'_{s\theta}\ V'_{s\theta}}. \tag{23}$$

The turbulence correlations labeled (i), (ii), (iii), (iv), (vi), (vii), (ix), and (x) all take the general form $\overline{V'_{si}\ S'}$, where S is any scalar quantity. Thus, these terms represent the transport of S by correlated fluctuations in velocity and the scalar quantity. As is typical, a gradient assumption is used to describe these turbulence correlations:

$$\overline{V'_{si}\ S'} = -\nu_{ts}\frac{\partial \bar{S}}{\partial x_i}. \tag{24}$$

The determination of ν_{ts}, as well as k_s and ϵ_s (term xii), will be addressed shortly. In addition, the turbulence correlation $\overline{\phi'_s\ T'}$ (terms viii and xi), which has no analogous single-phase counterpart, is simply retained in its present form; its significance will also be discussed later.

Using the simplifying assumptions and the modeling of the turbulence correlations described earlier, the governing equations are now applied to steady, fully developed flow in a vertical pipe. The equation of continuity for the gas phase, Eq. 10, reduces to

$$\frac{1}{r}\frac{d}{dr}\left[r\left(\overline{\phi_g}\,\overline{V_{gr}} - \nu_{ts}\frac{d\overline{\phi_g}}{dr}\right)\right] = 0. \tag{25}$$

Following integration, this equation is further simplified based on the requirement that the expression in curved brackets remains bounded as $r \to 0$:

$$\overline{V_{gr}} = \frac{\nu_{ts}}{\overline{\phi_g}}\frac{d\overline{\phi_g}}{dr}. \tag{26}$$

Similarly, the solid-phase equation of continuity, Eq. 11, takes the form:

$$\overline{V_{sr}} = \frac{\nu_{ts}}{\overline{\phi_s}}\frac{d\overline{\phi_s}}{dr}. \tag{27}$$

When the flow conditions and simplifying assumptions are applied to the gas-phase momentum balance (Eq. 12), both the axial and radial components are nontrivial. However, since the simplified forms of both components indicate that $\partial\bar{P}/\partial z$ is a constant, the solution of the radial component is not required. Hence, only the axial component of the gas-phase momentum balance is given below:

$$\rho_g \overline{V_{gr}}\frac{d\overline{V_{gz}}}{dr} = -\frac{\partial \bar{P}}{\partial z} - \beta\left(\overline{\phi_g}, \overline{V_{gj}}, \overline{V_{sj}}\right)\left(\overline{V_{gz}} - \overline{V_{sz}}\right). \tag{28}$$

The axial and radial components of the particle-phase momentum balance (Eq. 13) for the system under investigation are

$$0 = -\frac{1}{r}\frac{d}{dr}\left[r\left\{\sigma_{rz}\left(\overline{\phi_s}, \bar{T}, \overline{V_{si}}, \overline{V_{sj}}\right) - \rho_s\overline{\phi_s}\,\nu_{ts}\left(\frac{d\overline{V_{sz}}}{dr}\right)\right\}\right] + \rho_s\overline{\phi_s}g_z + \beta\left(\overline{\phi_g}, \overline{V_{gj}}, \overline{V_{sj}}\right)\left(\overline{V_{gz}} - \overline{V_{sz}}\right) \tag{29}$$

$$0 = -\frac{1}{r}\frac{d}{dr}\left[r\sigma_{rr}\left(\overline{\phi_s}, \bar{T}, \overline{V_{si}}, \overline{V_{sj}}\right)\right] + \frac{1}{r}\sigma_{\theta\theta}\left(\overline{\phi_s}, \bar{T}, \overline{V_{si}}, \overline{V_{sj}}\right) - \frac{\rho_s}{r}\frac{d}{dr}\left[r\overline{\phi_s}\left(\frac{2}{3}k_s - \overline{V_{sr}}\,\overline{V_{sr}}\right)\right] + \frac{\rho_s}{r}\overline{\phi_s}\left(\frac{2}{3}k_s\right) + \beta\left(\overline{\phi_g}, \overline{V_{gj}}, \overline{V_{sj}}\right)\left(\overline{V_{gr}} - \overline{V_{sr}}\right). \tag{30}$$

Equation 30 is further simplified by assuming that the normal components of the laminar solid-phase stress tensor σ_{ij} are isotropic (i.e., $\sigma_{rr} \approx \sigma_{\theta\theta}$). In addition, based on an order-of-magnitude analysis, $\overline{V_{sr}}\,\overline{V_{sr}} \ll \overline{V'_{sr}\ V'_{sr}} = (2/3)\,k_s$, and thus the second term in the square brackets of the radial momentum balance is neglected. Furthermore, as discussed by Dasgupta et al. (1994), the effect of the radial drag force, which is represented by the final term in Eq. 30, is secondary relative to that of the solid-phase Reynolds stress and is therefore ignored. With these simplifications, the radial component of the solid-phase momentum balance is written as

$$0 = -\frac{d}{dr}\left[\sigma_{rr}\left(\overline{\phi_s}, \bar{T}, \overline{V_{si}}, \overline{V_{sj}}\right) + \frac{2}{3}\rho_s\overline{\phi_s}\,k_s\right]. \tag{31}$$

Integrating the preceding expression results in the algebraic relation:

$$\sigma_{rr}\left(\overline{\phi_s}, \bar{T}, \overline{V_{si}}, \overline{V_{sj}}\right) + \frac{2}{3}\rho_s\overline{\phi_s}\,k_s = C, \tag{32}$$

where C is an integration constant.

The final governing equation to be applied to the vertical flow system is the pseudothermal energy balance (Eq. 14):

$$0 = -\frac{1}{r}\frac{d}{dr}\left[r\left\{q_r(\overline{\phi_s}, \bar{T}) - \frac{3}{2}\rho_s\,\nu_{ts}\,\overline{\phi_s}\frac{d\bar{T}}{dr}\right\}\right] - \sigma_{rr}\left(\overline{\phi_s}, \bar{T}, \overline{V_{si}}, \overline{V_{sj}}\right)\left(\frac{d\overline{V_{sr}}}{dr} + \frac{\overline{V_{sr}}}{r}\right) - \sigma_{rz}\left(\overline{\phi_s}, \bar{T}, \overline{V_{si}}, \overline{V_{sj}}\right)\left(\frac{d\overline{V_{sz}}}{dr}\right) - \gamma(\overline{\phi_s}, \bar{T}) - \frac{3}{2}\frac{\rho_s}{r}\frac{d}{dr}\left[r\,\overline{V_{sr}}\,\overline{\phi'_s T'}\right] + \rho_s\overline{\phi_s}\,\epsilon_s. \tag{33}$$

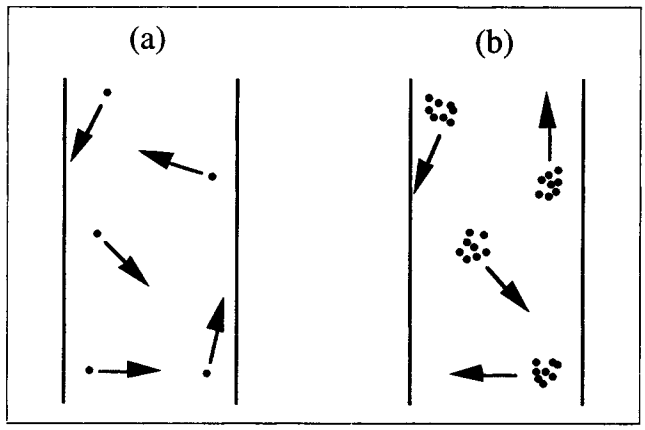

Figure 2. Regimes of gas–solid flows: (a) laminar and (b) turbulent.

The second last term in this equation is expected to be insignificant relative to the other terms due to the extremely small value of $\overline{V_{sr}}$. Although this term is omitted in Model 1, it will be included in the formulation of Model 2 wherein the modeling of $\overline{\phi_s' T'}$ is addressed. Hence, the pseudothermal energy balance takes the form:

$$0 = -\frac{1}{r}\frac{d}{dr}\left[r\left\{q_r(\overline{\phi_s}, \overline{T}) - \frac{3}{2}\rho_s \nu_{ts}\overline{\phi_s}\frac{d\overline{T}}{dr}\right\}\right] - \sigma_{rr}\left(\overline{\phi_s}, \overline{T}, \overline{V_{si}}, \overline{V_{sj}}\right)\left(\frac{d\overline{V_{sr}}}{dr} + \frac{\overline{V_{sr}}}{r}\right) - \sigma_{rz}\left(\overline{\phi_s}, \overline{T}, \overline{V_{si}}, \overline{V_{sj}}\right)\left(\frac{d\overline{V_{sz}}}{dr}\right) - \gamma(\overline{\phi_s}, \overline{T}) + \rho_s\overline{\phi_s}\,\epsilon_s. \quad (34)$$

At this point, a closer examination of the governing equations is useful. As mentioned earlier, two mechanisms exist that are responsible for the lateral segregation of solids. These two competing mechanisms are represented mathematically in the radial component of the solid-phase momentum balance (Eq. 32). The first term represents the laminar pressure while the second term represents the turbulent pressure. Recall that if the turbulent pressure dominates, the correct solids concentration profile will be obtained. However, it is interesting to note that even if the laminar pressure is significantly larger than turbulent pressure, the undue sensitivity to inelastic particle–particle collisions may still be eliminated due to the presence of the two terms associated with particle-phase turbulence in the pseudothermal energy balance (Eq. 34). In particular, the turbulent conduction, which is represented by the second term in square brackets, will tend to flatten the granular temperature profile in the core of the pipe, resulting in a corresponding decrease in the solids concentration near the pipe center (see Figures 1 and 2, e = 0.99). Likewise, the final term in Eq. 34, which represents the additional source of pseudothermal energy, will have the same effect. As a result, if the magnitude of either of these terms is large enough, the extreme sensitivity to the coefficient of restitution will be removed. Thus, the treatment used to develop Model 1, namely the time-averaging of only the governing equations, may be sufficient for the prediction of qualitatively correct segregation patterns regardless of whether the laminar or turbulent mechanism dominates.

In order to make the governing equations explicit, relations for both the kinetic theory expressions and the turbulence quantities ν_{ts}, k_s, and ϵ_s are needed. The kinetic theory expressions adopted in this work, which are given in Table 2, are slightly modified forms of the relations derived by Lun et al. (1984). The modifications, which are needed in order to account for the presence of bounding walls, are based on the proposal of Louge et al. (1991). Strictly speaking, the expression for σ_{rr} contains additional terms involving the radial solids velocity. The same is true for $\sigma_{\theta\theta}$, though the additional terms are not identical to the corresponding terms of σ_{rr}. However, for the broad range of conditions studied here,

Table 2. Kinetic Theory Expressions for σ_{ij}, q_i, and γ

Solid-phase stresses

$$\sigma_{rr} = \sigma_{\theta\theta} = \rho_s T\left(\frac{\phi_s}{1+\lambda_{mfp}/R} + 4\eta\phi_s^2 g_o\right)$$

$$\sigma_{rz} = -\mu_s\frac{dV_{sz}}{dr} = -\rho_s\,\phi_s\,\nu_s\frac{dV_{sz}}{dr}$$

$$\mu_s = \frac{5\sqrt{\pi}}{96}\rho_s d_p\sqrt{T}\left[\left(\frac{1}{1+\lambda_{mfp}/R}\,\frac{1}{\eta g_o} + \frac{8\phi_s}{5}\right)\left(\frac{1+\frac{8}{5}\eta(3\eta-2)\phi_s g_o}{2-\eta}\right) + \frac{768}{25\pi}\eta\phi_s^2 g_o\right]$$

Flux of pseudothermal energy

$$q_r = -\frac{25\sqrt{\pi}}{128}\rho_s d_p\sqrt{T}\left[\left(\frac{1}{1+\lambda_{mfp}/R}\,\frac{8}{\eta g_o} + \frac{96\phi_s}{5}\right)\left(\frac{1+\frac{12}{5}\eta^2(4\eta-3)\phi_s g_o}{41-33\eta}\right) + \frac{512}{25\pi}\eta\phi_s^2 g_o\right]\frac{\partial T}{\partial r}$$

Dissipation of pseudothermal energy

$$\gamma = \frac{48}{\sqrt{\pi}}\frac{\rho_s}{d_p}\eta(1-\eta)\phi_s^2 g_o T^{3/2}$$

$$\lambda_{mfp} = \frac{d_p}{6\sqrt{2}\,\phi_s} \qquad \eta = \frac{1}{2}(1+e) \qquad g_o = \frac{\phi_{so}^{1/3}}{\phi_{so}^{1/3} - \phi_s^{1/3}}$$

these extra terms are found to be orders of magnitude smaller than the term shown in Table 2, which is common to both σ_{rr} and $\sigma_{\theta\theta}$. Hence, the assumption of the isotropy of the normal components of σ_{ii} is valid.

Similar to single-phase flows, the complexity of the description chosen for ν_{ts}, as well as k_s and ϵ_s, is based on the nature of the flow under consideration. Since the system of interest here is fully developed flow in a vertical pipe, a simple mixing-length-type closure is proposed:

$$\nu_{ts} = l_{ms}^2 \left| \frac{d\overline{V_{sz}}}{dr} \right|, \tag{35}$$

where l_{ms} is the mixing length. Note that the eddy viscosity should also contain terms involving the radial solids velocity; however, similar to the normal component of the laminar solid-phase stresses, these terms are small enough relative to $d\overline{V_{sz}}/dr$ to be ignored.

This mixing-length treatment is chosen based on the analogy that is being made between single-phase turbulence and particle-phase turbulence. Namely, it is believed that the mechanical interactions responsible for turbulence in single-phase flows are similar to the interactions that govern particle-phase turbulence. It is important to note, however, that models for single-phase turbulent flows do contain a certain amount of empiricism and that this empiricism is not expected to be the same for single-phase flows as for gas–solid flows. Nevertheless, since the primary focus of this work is to determine the physical mechanism that is responsible for the particle segregation patterns observed in vertical pipe flow, a mixing length model with single-phase turbulence constants is used as a first and somewhat crude attempt at closure. Accordingly, the following expressions are implemented:

$$l_{ms} = R\left[0.14 - 0.08\left(\frac{r}{R}\right)^2 - 0.06\left(\frac{r}{R}\right)^4\right]\left(1 - \frac{\overline{\phi_s}}{\phi_{so}}\right) \tag{36}$$

$$k_s = \left(\frac{\nu_{ts}}{l_{ms}\, c_D^{1/4}}\right)^2 \tag{37}$$

$$\epsilon_s = \frac{c_D^{3/4}\, k^{3/2}}{l_{ms}}, \tag{38}$$

where R is the pipe radius; ϕ_{so} is the solids volume fraction at closest packing; and $c_D = 0.08$ as is typical for single-phase turbulent flows. The description of the mixing length appearing in Eq. 36 is the typical Nikuradse mixing length multiplied by a damping function. The damping function is employed in order to predict the diminishing effects of particle-phase turbulence as high solids packings are approached; this trend has been observed in both experiments and simulations of granular flows (Savage and Sayed, 1984; Hopkins and Louge, 1991; Walton et al., 1991).

In its present form, the description of the eddy viscosity as it appears in Eq. 35 is not adequate. Since the solids velocity gradient at the pipe center line is zero, this equation indicates that the eddy viscosity will also equal zero. Thus, the diffusive nature of turbulence is not taken into consideration. For single-phase turbulent flows, the ramifications of such a description are typically unimportant since the Reynolds stress, which is defined as proportional to the eddy viscosity, also approaches zero toward the pipe center. Although the same is true for the particle-phase Reynolds stress, the turbulent kinetic energy of the solid phase should not approach zero at the center line, as is dictated by Eq. 37. Thus, if this treatment of the eddy viscosity is used, k_s will reach a minimum both at the pipe center line and at the pipe wall, and thus the turbulent mechanism for particle segregation will show a concentration of particles at both locations. Hence, a correction is needed to reflect the known behavior of the turbulent kinetic energy, namely that k_s reaches a minimum at the pipe wall only. In order to propose such a correction, attention is again given to single-phase, turbulent pipe flow. Experimental measurements of such flows have shown that a universal profile of the eddy viscosity exists (see, for example, Myong and Kasagi, 1990). In particular, the center-line value of the eddy viscosity is typically 0.85 of its highest value. This universality is now applied to ν_{ts} in order to ensure that it does not vanish at the pipe center. First, Eq. 35 is used to determine the eddy viscosity across the entire flow domain. Based on the obtained profile, the value (ν_{ts}^*) and location (r^*) of the maximum eddy viscosity is determined. A third-order polynomial fitted to satisfy the conditions listed below is then used to describe the behavior of the eddy viscosity between $r = 0$ and $r = r^*$:

$$\nu_{ts}(r=0) = 0.85\ \nu_{ts}^*; \qquad \frac{d\nu_{ts}}{dr}(r=0) = 0 \tag{39}$$

$$\nu_{ts}(r=r^*) = \nu_{ts}^*; \qquad \frac{d\nu_{ts}}{dr}(r=r^*) = 0. \tag{40}$$

Finally, to complete the formulation of the model, boundary conditions both at the pipe axis and wall are required for $\overline{V_{gz}}$, $\overline{V_{sz}}$, and T. Due to the axisymmetrical nature of the flow, the gradient of each of these variables is forced to zero at the pipe center line. Although the point velocity of the gas phase is zero at the solid boundary, $\overline{V_{gz}}$ represents a locally averaged variable and is thus nonzero at the wall. However, for the high solids loadings considered in this work, the averaging region is extremely small, and thus the approximation $\overline{V_{gz}} = 0$ is used for the wall boundary condition. Depending on the smoothness of the pipe surface, the solid particles may slip at the wall. Pita and Sundaresan (1991) showed, however, that the boundary condition implemented by Johnson and Jackson (1987) reduces to $\overline{V_{sz}} \approx 0$ for small particles similar to those investigated in this study. Hence, the no-slip condition for the particle velocity is used here. The boundary condition for the pseudothermal temperature is based on a balance of pseudothermal energy at the pipe wall. For the system under consideration, the conduction of pseudothermal energy to the wall equals the energy lost at the wall due to inelastic particle–wall collisions:

$$q_r(\overline{\phi_s}, \overline{T}) = \frac{\sqrt{3}\ \rho_s\, \pi(1-e_w^2)\, \overline{T}^{3/2}}{4\left(\frac{\phi_{so}}{\overline{\phi_s}} - \frac{\phi_{so}^{2/3}}{\overline{\phi_s}^{2/3}}\right)}. \tag{41}$$

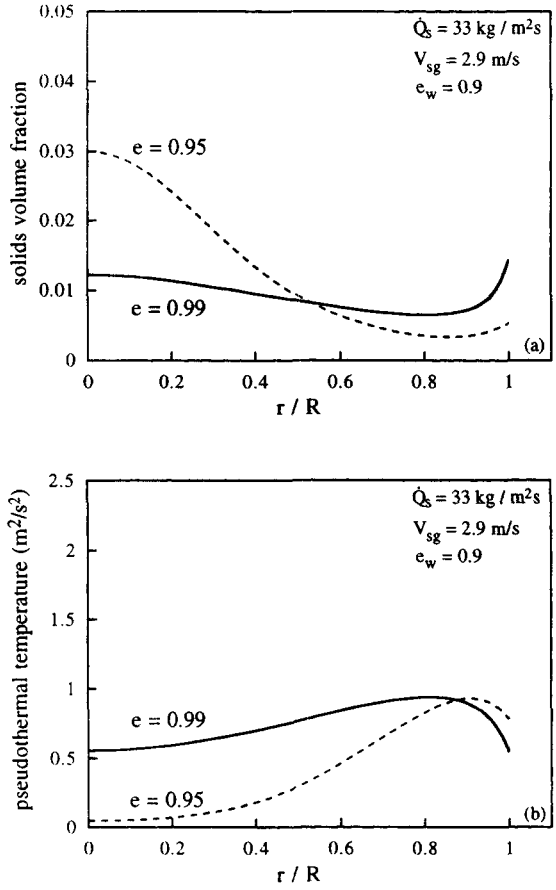

Figure 3. Model 1: radial variation of (a) solids volume fraction and (b) pseudothermal temperature for conditions in Table 1.

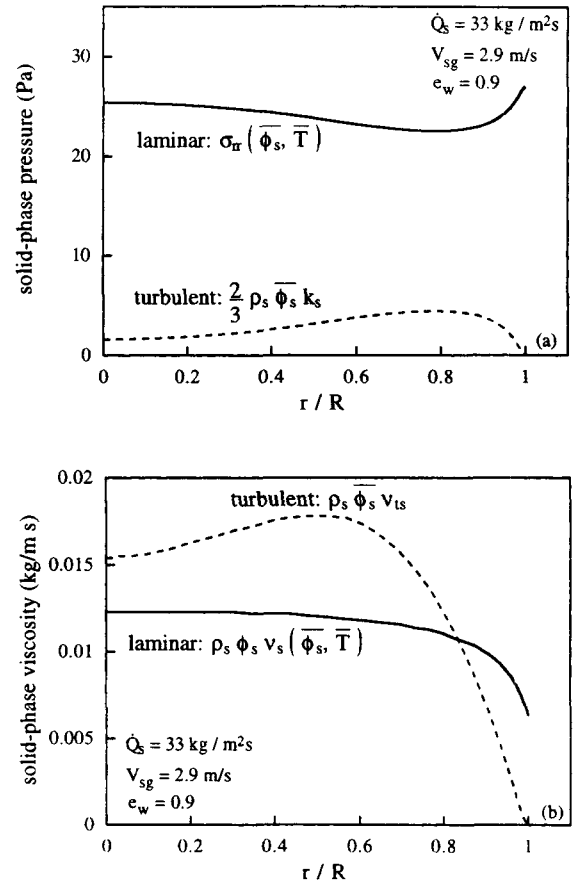

Figure 4. Model 1: radial variation of solid-phase (a) pressure, and (b) viscosity for conditions in Table 1.

Assessment of Model 1. The governing set of continuity, momentum, and fluctuation energy balances is given by three second-order differential equations (Eqs. 28, 29 and 34) and four algebraic relations (Eqs. 9, 26, 27 and 32). Using the algebraic relations to eliminate four of the seven variables ($\overline{\phi_g}$, $\overline{\phi_s}$, $\overline{V_{gr}}$, $\overline{V_{sr}}$, $\overline{V_{gz}}$, $\overline{V_{sz}}$, and T) from the differential equations results in a system of three differential equations in three unknowns subject to two-point boundary conditions. This system was solved using an adaption of the control-volume technique proposed by Patankar (1980). In this method, integration of the "pseudo-transient" system continues until the steady-state solution is reached. The sensitivity of the results to the 60-point, nonuniform radial grid was checked by making certain that increasing the number of points had a negligible effect on the computed profiles.

The ability of Model 1 to predict the segregation patterns characteristic of dense-phase flows is exemplified in Figures 3 and 4. The system parameters corresponding to these figures are given in Table 1. Figures 3a and 3b depict the radial variation in the solids volume fraction and pseudothermal temperature, respectively, for two different particle–particle coefficients of restitution, $e = 0.99$ and $e = 0.95$. When comparing these results with the results of the Sinclair and Jackson (1989) model shown in Figure 1 for the same conditions, it is concluded that the "turbulent" model is less sensitive to the inelasticity of particle–particle collisions than the "laminar" model. In particular, Model 1 predicts a segregation of particles at the pipe wall for $e = 0.99$, while the Sinclair and Jackson (1989) Model shows a rather high concentration of solids at the center of the pipe. At $e = 0.95$, however, Model 1 also exhibits a segregation of particles in the core of the pipe. Thus, although Model 1 is less sensitive to inelastic particle–particle collisions than models that do not account for particle-phase turbulence, the undue sensitivity has not been eliminated.

As explained previously, this sensitivity remains because the laminar contribution to the solid-phase pressure is larger than the turbulent contribution. The difference between the two contributions is displayed in Figure 4a. Evidently, the extra terms present in the pseudothermal energy balance (Eq. 34) that are associated with particle-phase turbulence, namely the turbulent conduction and additional source of pseudothermal energy, are not large enough to counterbalance the large sink due to inelastic particle–particle collisions. Thus, the drop in pseudothermal energy at the pipe center as plotted in Figure 3b for $e = 0.95$ results in a corresponding increase in the solids volume fraction. In addition, although not shown here, as the solids loading of this system is increased, the difference between the two contributions to the solid-phase pressure increases, thereby heightening the sensitivity to e at higher solids loadings.

Also noteworthy is the difference in the contributions to

the solid-phase viscosity found in the axial component of the solid-phase momentum balance (Eq. 29) as presented in Figure 4b. Unlike the contributions to the solid-phase pressure, the *turbulent* contribution to the solid-phase viscosity is greater than the laminar contribution over most of the flow domain. Again, this difference is found to increase as the solids concentration of this system is increased. Similar to single-phase flows, this increase in the turbulent viscosity relative to the laminar viscosity leads to a flattening of mean variable profiles. As shown in Figures 5a and 5b, however, the amount of flattening is unrealistic. In these figures, model predictions are compared with the experimental data obtained by Bader et al. (1988), for which the system conditions are specified in Table 3. In order to highlight the effects of the difference in the contributions to the solid-phase viscosity, rather than those of the solid-phase pressure, model predictions were obtained for $e = 1.0$ and $e_w = 0.9$. The adverse effects of this behavior are most apparent in Figure 5a, in which the predicted solids flux profile is flattened to the point where no solids downflow is present, whereas a considerable amount of downflow was measured experimentally. Similarly, as depicted in Figure 5b, the segregation of solids at the pipe wall as obtained by the model is much smaller than that of the experimental data.

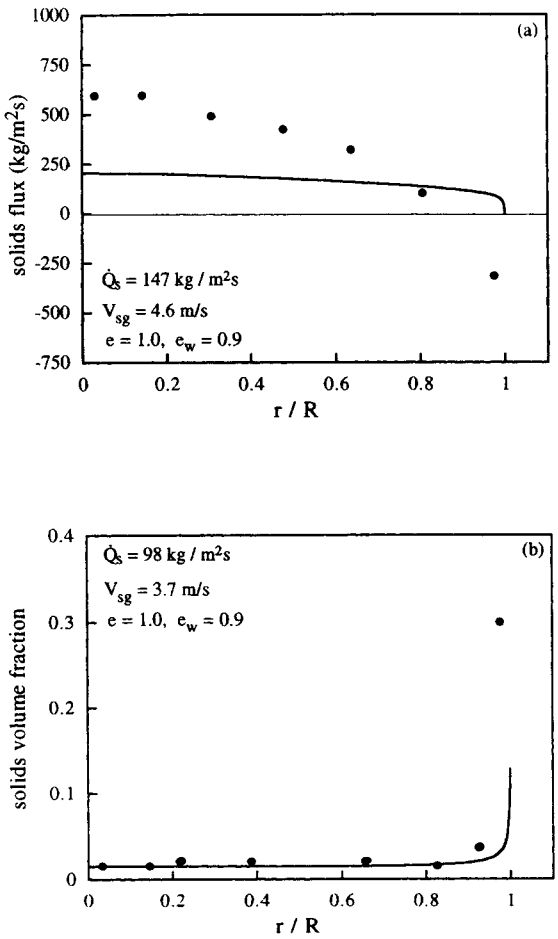

Figure 5. Model 1 vs. experimental data of Bader et al. (1988): radial variation of (a) local solids flux, and (b) solids volume fraction.

Table 3. Summary of System Parameters for Published Experimental Data Sets*

Reference	D (cm)	L/D	d_p (μm)	ρ_s (kg/m^3)
Weinstein et al. (1986)	15.2	31	59	1,460
Yerushalmi (1986)	15.2	41	49	1,070
Bader et al. (1988)	30.5	30	76	1,714
Rhodes et al. (1988)	15.2	28	64	1,800
Harris et al. (1993)	14.0	29	60	1,700

*The values $\rho_g = 1.2$ kg/m^3, $\mu_g = 1.81 \times 10^{-5}$ kg/m·s, and $\phi_{so} = 0.65$ are assumed for each data set.

At this point, then, two unrealistic behaviors exist that need to be further addressed. First, the model still manifests an excessive sensitivity to inelastic particle–particle collisions since the *laminar* contribution to the solid-phase pressure is greater than the turbulent contribution. In addition, the model predictions of the mean variable profiles are overly flat due to the fact that the *turbulent* contribution to the viscosity is larger than its laminar counterpart. As alluded to earlier, one possible explanation for these behaviors is the appropriateness of the single-phase turbulence constants to describe the phenomena of particle-phase turbulence. As expected, however, the "tuning" of these constants cannot alleviate both of these problems simultaneously. In particular, an adjustment of single-phase turbulence parameters would result in either an increase in the turbulent contribution to *both* the solid-phase pressure and viscosity over the corresponding laminar contributions or vice versa. As a result, only one of the two aforementioned behaviors would be resolved, while the effects of the other would worsen.

Another key issue that may be related to the two incorrect behaviors and is not accounted for in the framework of the present model is the effect of particle-phase turbulence on the kinetic theory expressions. As mentioned earlier, the kinetic theory expressions are derived assuming smoothly varying flow fields, and thus, strictly speaking, are not applicable to flows in which particle packets are present. In order to gauge the effects of this assumption on such flows, a more detailed consideration of the kinetic theory closures is needed.

Model 2: effects of particle-phase turbulence on the kinetic theory closures

In order to account for the effects of particle-phase turbulence on the kinetic theory expressions, the closures can be linearized and then time-averaged in a manner similar to the governing equations. However, even after linearizing these expressions, the time-averaging gives rise to a number of complicated turbulence correlations. Since the physical interpretation *alone* of these terms is extremely difficult, the required modeling of the correlations would be speculative at best. For this reason, attention here is focused on the kinetic theory expression that describes the effects of inelastic particle–particle collisions and is thus associated with the excessive sensitivity of the model to e, namely the dissipation of pseudothermal energy γ (i.e., when $e = 1.0$, $\gamma = 0$; when $e < 1.0$, this sink term is "turned on" and an unrealistic drop in the pseudothermal temperature at the pipe core is predicted).

Prior to time-averaging the kinetic theory expression for γ, a linear approximation of this dissipation term is made in order to simplify the form of the resulting turbulence correlations. Given the representation:

$$\gamma = \frac{\rho_s}{d_p} f_1(\phi_s) f_2(T), \tag{42}$$

where the functional forms of f_1 and f_2 can be inferred from Table 2, γ is approximated using the expression

$$\gamma \approx \frac{\rho_s}{d_p}\left[f_1(\overline{\phi}_s) + \left(\frac{\partial f_1}{\partial \phi_s}\right)_{\overline{\phi}_s} \phi_s'\right]\left[f_2(\overline{T}) + \left(\frac{\partial f_2}{\partial T}\right)_{\overline{T}} T'\right]. \tag{43}$$

Based on the preceding relation, the time-averaged form of the dissipation due to inelastic particle–particle collisions is given by

$$-\overline{\gamma} = \frac{\rho_s}{d_p}\left[-f_1(\overline{\phi}_s) f_2(\overline{T}) - \left(\frac{\partial f_1}{\partial \phi_s}\right)_{\overline{\phi}_s}\left(\frac{\partial f_2}{\partial T}\right)_{\overline{T}} \overline{\phi_s' T'}\right]. \tag{44}$$

The first term on the righthand side of this equation is the same expression (see Eq. 8) that was utilized in Model 1 to describe the sink of pseudothermal energy due to inelastic particle–particle collisions. Again, this term, which is always negative in sign, is responsible for the excessive drop in pseudothermal temperature when $e < 1.0$. The sign of the second term in square brackets, however, depends on the sign of the turbulence correlation since the two partial derivatives are always positive quantities. The sign of this correlation can be deduced by considering the nature of a particle packet present in a gas–solid flow system. First, the solids volume fraction within a particle cloud is larger than its average value outside the cloud. Due to the increased number of *inelastic* particle collisions within the cloud, the pseudothermal temperature in the cloud interior is expected to be smaller than its exterior counterpart, as was observed in the gas–solid flow simulations of Tsuji et al. (1994). Thus, the time-averaged correlation between the fluctuating solids volume fraction and pseudothermal temperature is always a negative quantity. As a result, the second term on the righthand side of Eq. 44 acts as an additional source of pseudothermal energy, and thus may be capable of offsetting the dissipation of pseudothermal temperature associated with the first term in square brackets.

Before the effects of particle-phase turbulence on the kinetic theory expression for γ, as represented by Eq. 44, can be included in the model, a closure relation for $\overline{\phi_s' T'}$ is required. Since the behavior of this correlation has not been addressed in the literature, the modeling of this term is based on the physical picture of the gas–solid flow system that has been presented. More specifically, as the intensity of particle-phase turbulence increases, the magnitude of the turbulence correlation is expected to increase as well. In addition, since particle packets are most prevalent at moderate solids concentrations, the absolute value of the correlation is anticipated to be largest in the core of the pipe and decrease as the wall is approached. Based on these two behaviors, the following closure is proposed:

$$\overline{\phi_s' T'} \propto (\overline{\phi}_s)_{\text{avg}}\, k_{s,\text{avg}}\left[(\phi_{so} - \overline{\phi}_{s,w} - 1)(r/R)^n + 1\right], \tag{45}$$

where the subscript avg refers to the average value of a given quantity across the pipe radius and the subscript w refers to the value of a given quantity at the pipe wall. The first two quantities on the righthand side of Eq. 45 represent the average turbulent intensity of the solid phase. These two quantities are solely responsible for the magnitude of the turbulence correlation, since the term in square brackets controls only the shape of the correlation. In particular, the function defined within these brackets, which is symmetrical about $r = 0$, is equal to unity at the pipe centerline and $\phi_{so} - \overline{\phi}_{s,w}$ at the pipe wall. Hence, the shape of $\overline{\phi_s' T'}$ becomes steeper as the solids concentration at the wall increases, as is expected in the dense-phase regime. Although this steepening behavior of the shape function is not true in the packed-bed limit, the value of the turbulent intensity does go to zero at $\overline{\phi}_s = \phi_{so}$, and thus the correct limiting value is obtained.

In order to implement the closure relation for $\overline{\phi_s' T'}$ (Eq. 45), values are needed for the constant of proportionality and the exponent n, where n dictates the flatness of the correlation profile in the core region of the pipe. The values assigned here are -5 and 8, respectively, based on a comparison of model predictions with experimental data. Again, the constant of proportionality is negative in sign since, as previously discussed, the turbulence correlation between the fluctuating solids concentration and pseudothermal temperature is a negative quantity. Although this particular treatment of $\overline{\phi_s' T'}$ is a somewhat speculative first attempt at closure, it is important to emphasize that it does capture the expected behavior of the turbulence correlation.

The governing system of equations for Model 2 is identical to that of Model 1, with the main exception that the dissipation of pseudothermal energy $\gamma(\overline{\phi}_s, \overline{T})$ is replaced by its time-averaged value as defined in Eq. 44. In addition, the term present in the pseudothermal energy balance (second term from right in Eq. 33), which involves the $\overline{\phi_s' T'}$ correlation and is not included in the formulation of Model 1, is reintroduced. Hence, Eq. 33, rather than Eq. 34, is used to ensure a balance of pseudothermal energy. It should be noted, however, that the effects of the $\overline{\phi_s' T'}$ term are indeed found to be negligible over the wide range of conditions investigated in this work. Finally, the mixing length utilized in Model 2 is taken to be one-fourth of the value prescribed in Eq. 36, based on comparisons with available data.

A quick gauge as to the predictive ability of the model just described (Model 2) compared to that of the model that does not account for the effects of particle-phase turbulence on the kinetic theory expressions (Model 1) is portrayed in Figures 6a and 6b. In these figure parts, the predictions of Model 2 obtained using $e = e_w = 0.9$ are compared with the local solids flux and solids volume fraction measurements of Bader et al. (1988). A comparison of these predictions with the corresponding predictions of Model 1 for $e = 1.0$ and $e_w = 0.9$ (Figures 5a and 5b) reveals that *both* of the unrealistic behaviors associated with Model 1 are no longer present. First, as exhibited in Figure 6b, Model 2 predicts particle segregation at the pipe wall for a particle–particle coefficient of restitution that is significantly less than unity. Although not shown, this segregation results even though the laminar pressure is dominant, thereby implying that the extra production of

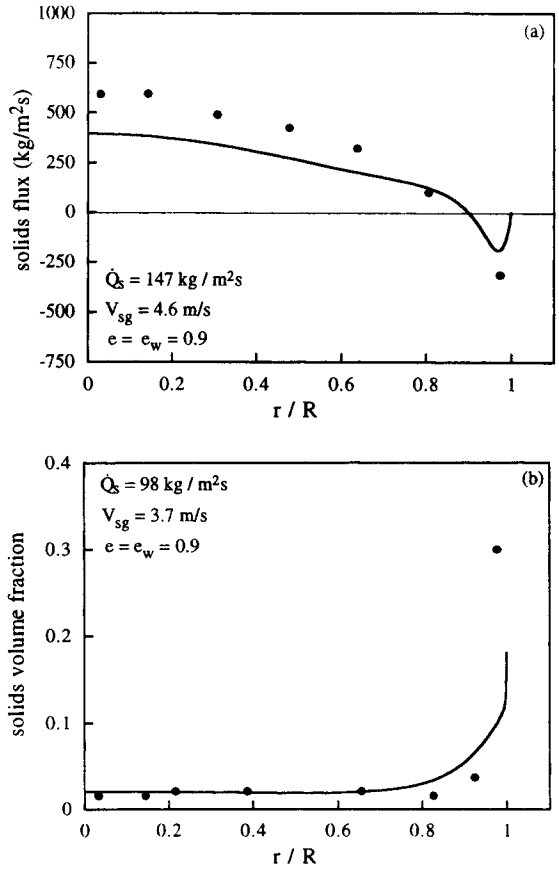

Figure 6. Model 2 vs. experimental data of Bader et al. (1988): radial variation of (a) local solids flux, and (b) solids volume fraction.

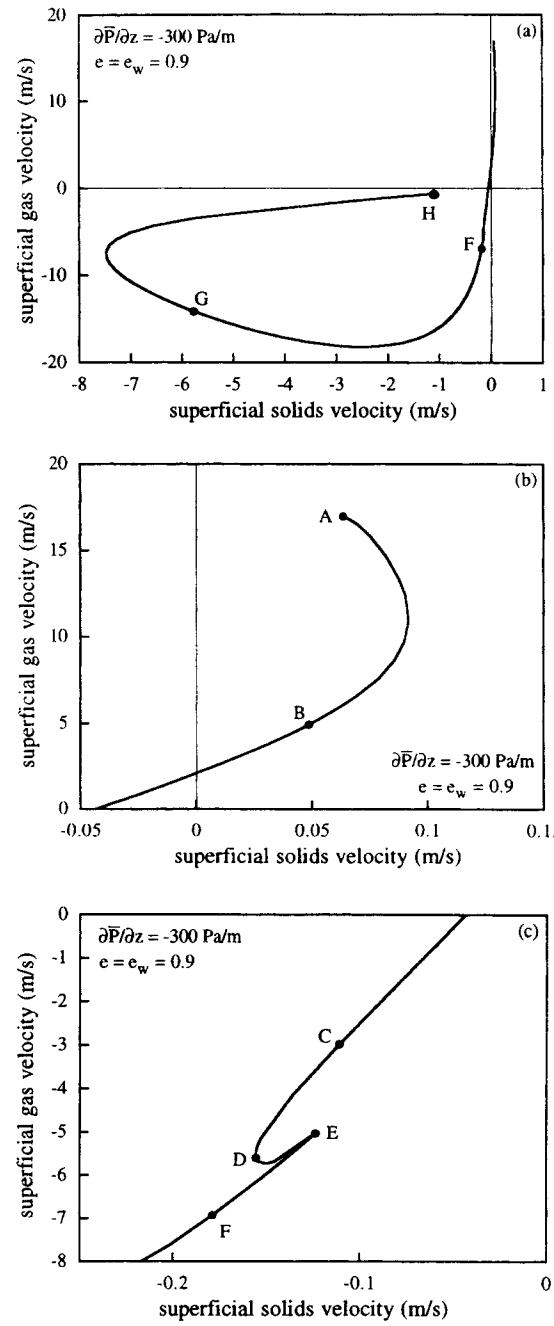

Figure 7. Model 2: contour of constant pressure gradient in (a) all quadrants, (b) first and second quadrants, and (c) portion of third quadrant of V_{ss}-V_{sg} plane.

pseudothermal energy associated with $\overline{\phi_s' T'}$ is large enough to counterbalance the sink due to inelastic collisions. Moreover, the undue flattening of the mean variable profiles as demonstrated by Model 1 (Figures 5a and 5b) is not apparent in the predictions of Model 2. As displayed in Figure 6a, Model 2 predicts the downflow of particles at the wall, though not to the extent of the experimental data, whereas Model 1 shows upflow across the entire pipe radius (Figure 5a). Based on these results, it appears that the mechanical interaction necessary for the prediction of realistic flow patterns has been isolated, and thus a comprehensive investigation of the predictive ability of Model 2 is warranted.

Presentation and Discussion of Results

To further assess the capabilities of Model 2, the qualitative nature of its predictions over a wide range of operating conditions is examined and comparisons with available experimental data are made. For each of the cases considered, model predictions were obtained using $e = e_w = 0.9$.

Figure 7a, which relates the superficial gas velocity (V_{sg}) to the superficial solids velocity (V_{ss}) for a constant axial pressure gradient of -300 Pa/m, gives a general picture of the gas–solid flow behavior predicted by Model 2. The portions of this contour that are difficult to decipher on the scale in Figure 7a are shown with expanded scales in Figures 7b and 7c. Table 4 lists the system parameters used to obtain these plots. (In an effort to facilitate potential comparisons between different published models, the parameter values chosen are identical to those implemented by Dasgupta et al., 1995.) Note that the constant pressure gradient curve predicted by the model passes through each of the first three quadrants, which represent cocurrent upflow, countercurrent flow, and cocurrent downflow, respectively. The radial profiles of the solids velocity and solids volume fraction corresponding to various points marked along the pressure

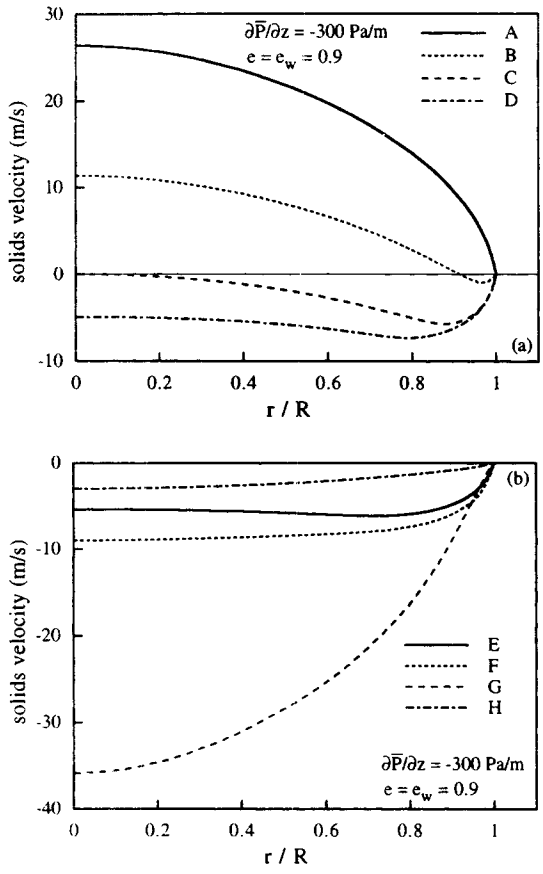

Figure 8. Model 2: radial variation of solids velocity at points (a) *A* to *D* and (b) *E* to *F* in Figure 7.

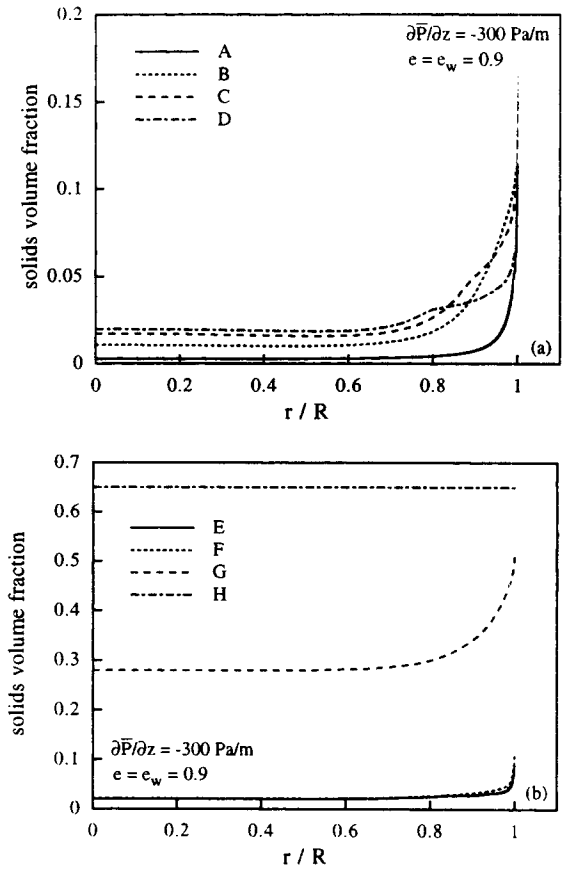

Figure 9. Model 2: radial variation of solids volume fraction at points (a) *A* to *D* and (b) *E* to *F* in Figure 7.

gradient contour are presented in Figures 8 and 9, respectively.

The system of lowest solids loading along the predicted curve is labeled A (Figure 7a). Although the prediction obtained by a model valid in the dilute limit would continue upward and meet the V_{sg} axis at zero solids loading, more dilute flows were not attempted with the current model since gas-phase diffusion, which plays an important role in dilute-phase flows, is neglected. As is apparent in Figure 8a, all of the solid particles in the system represented by point *A* are flowing upward across the tube radius. Upon moving down the fixed-pressure-gradient contour, the overall solids concentration of the system increases, and the maximum attainable superficial solids velocity as predicted by the model is encountered. This transitional point corresponds to the onset of particle downflow. As portrayed in Figure 8a, the denser system at point *B* exhibits an upflow of particles in the pipe core and a downflow of particles near the pipe wall due to the increased particle segregation (Figure 9a). The overall solids concentration continues to increase as the pressure-gradient contour passes from the first to second quadrant, at which time a net downflow of solids occurs, while a net upflow of gas is maintained. A net downflow of both phases is present in the third quadrant and the contour remains in the third quadrant as the system becomes increasingly denser.

As indicated by the expanded portion of the third quadrant displayed in Figure 7c, three superficial gas velocities that are relatively close in value are predicted to exist for a given superficial solids velocity. Although the exact source of this multiplicity is difficult to pinpoint due to the tightly coupled nature of the flow variables, it is interesting to note, though not shown here, that the laminar and turbulent contribution to the viscosity are roughly equal in magnitude in this region. Elsewhere along the contour, the laminar contribution is dominant. (Radial profiles of these and other relevant flow quantities are detailed by Hrenya, 1996.)

Continuing along the constant pressure gradient curve from this region of multiplicity, the superficial solids velocity continues to decrease until the global minimum is reached. Past this minimum, the amount of radial segregation is still large, as seen in Figure 9b for the system represented by point *G*. Further along, the lowest possible superficial gas velocity is attained. In this region, both the solids velocity and solids concentration profiles begin to flatten rapidly through point *H* as the packed-bed limit is approached.

Similar plots in the $V_{ss}-V_{sg}$ plane are given in Figure 10a for three different values of fixed axial pressure gradient: -100 Pa/m, -500 Pa/m, and $-1{,}000$ Pa/m. The other system parameters used for model calculations remain unchanged (Table 4). As expected, a decrease in the pressure gradient results not only in an increase in the choking velocity (first quadrant), but also in an increase in the minimum superficial gas and solids velocities (third quadrant). Figure 10b shows an enlargement of the second quadrant with the addition of several constant-pressure gradient curves. These

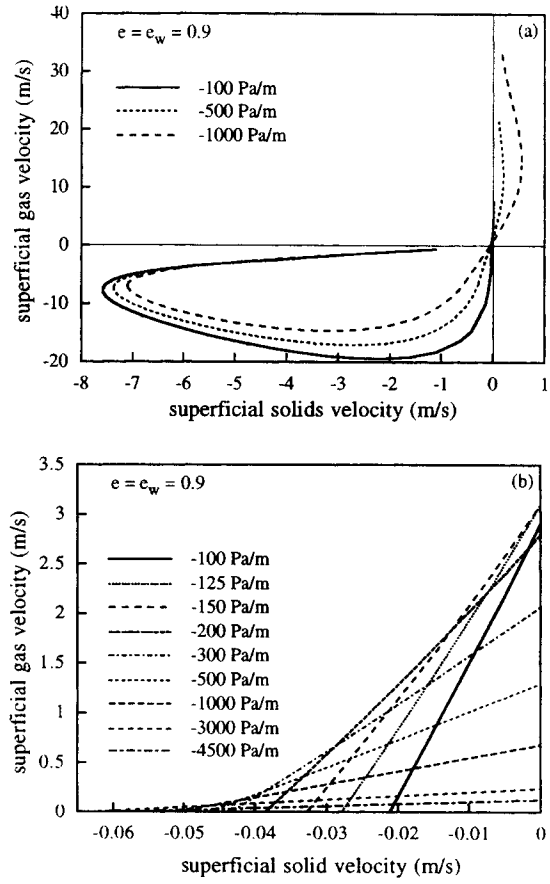

Figure 10. Model 2: contours of various constant pressure gradients in (a) all quadrants, and (b) second quadrant of V_{ss}-V_{sg} plane.

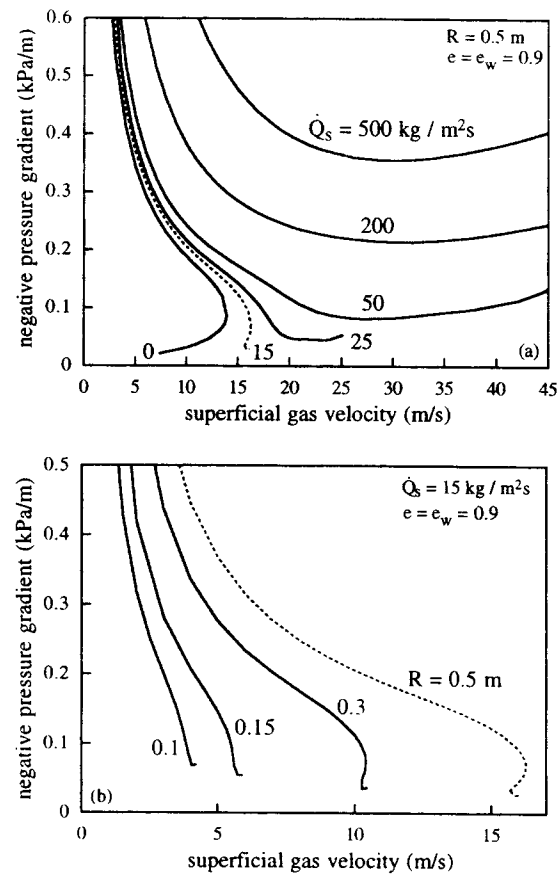

Figure 11. Model 2: contours in the $\partial\bar{P}/\partial z$-$V_{sg}$ plane for (a) various overall solids fluxes, and (b) various pipe radii.

curves form the well-known flooding envelope, which outlines the range of operating conditions possible in the countercurrent flow regime.

This overall picture of the flow behavior just summarized is similar to that obtained by the model of Sinclair and Jackson (1989) and is consistent with the qualitative nature known to vertical gas–solid flows. For the Sinclair and Jackson (1989) model, however, the $V_{ss}-V_{sg}$ flow map was constructed using $e = 1.0$ and $e_w = 0.9$; similar plots could not be constructed even for $e = 0.99$ due to the extreme sensitivity of the model to inelastic particle–particle collisions. On the other hand, the predictions of the present model, which were obtained for collisions characterized by $e = e_w = 0.9$, show the expected radial segregation patterns over the entire range of flow conditions. Furthermore, these segregation patterns are predicted even though the laminar contribution to the solid-phase pressure is significantly larger than its turbulent counterpart everywhere along the contour (Hrenya, 1996). Evidently, the additional source of the pseudothermal energy arising from the time-averaging of γ, as described by Eqs. 44 and 45, is able to effectively counterbalance the sink predicted by the original kinetic-theory expression.

Another performance diagram that is useful in assessing the predictive ability of the model and is probably of more practical use than the $V_{ss}-V_{sg}$ flow map is the well-known Zenz diagram, which relates the axial pressure gradient to the superficial gas velocity for a system of constant overall solids flux. The model predictions for this relationship are plotted in Figure 11a for several values of solids flux. Table 5 specifies the system parameters used in the model simulations. (Again, in order to facilitate comparisons between different models, the values chosen are the same as those utilized by Pita and Sundaresan (1991) to examine the scale-up characteristics of the Sinclair and Jackson, 1989 model.) The relationship between $\partial\bar{P}/\partial z$ and V_{sg} predicted by the current

Table 4. System Parameters for V_{ss}-V_{sg} Plots at Constant $\partial\bar{P}/\partial z$ (Figures 7–10)

Pipe diameter (D)	30 cm
Particle diameter (d_p)	100 μm
Particle density (ρ_s)	1,500 kg/m^3
Gas density (ρ_g)	1 kg/m^3
Gas viscosity (μ_g)	4×10^{-5} kg/m·s
Solids volume fraction at closest packing (ϕ_{so})	0.65

Table 5. System Parameters for Zenz Diagrams (Figure 11)

Pipe diameter (D)	1 m
Particle diameter (d_p)	70 μm
Particle density (ρ_s)	1,500 kg/m^3
Gas density (ρ_g)	1.22 kg/m^3
Gas viscosity (μ_g)	4×10^{-5} kg/m·s
Solids volume fraction at closest packing (ϕ_{so})	0.65

model exhibits the expected U-shape for systems of large solids flux. To the left of the minimum, the required pressure gradient increases as V_{sg} decreases due to the increased weight of the suspension, whereas to the right, the required pressure gradient increases with V_{sg} due to the increased frictional losses at the pipe wall. However, for systems of relatively small overall solids flux, a region exists where more than one value of the pressure gradient is associated with a system of given V_{sg} and $\dot{Q}_s$. The existence of such a multiplicity has been frequently observed in practice (e.g., Yerushalmi and Avidan, 1985). Although a similar behavior was predicted by Pita and Sundaresan (1991), perfectly elastic particle–particle collisions had to be assumed in order to obtain the results.

The effect of the riser diameter on the relation between $\partial \bar{P}/\partial z$ and V_{sg} is presented in Figure 11b for the same set of system parameters (Table 5). All of the model predictions seen here correspond to a constant solids flux of 15.0 kg/(m^2·s), and hence the broken lines in Figures 11a and 11b represent the same system. As is apparent from this graph, the model predicts that the region of multiplicity disappears as the tube diameter decreases. Thus, the scale-up of systems operating in this range is not straightforward, as the existence of the multiplicity depends on both the overall solids flux (Figure 11a) and the pipe size (Figure 11b).

As mentioned earlier, the overall goal of this modeling effort has been to gain a more thorough understanding of the mechanisms responsible for particle segregation observed in vertical pipe flow. Hence, the focus up to this point has been on the qualitative nature of the model predictions. Because the model is able to predict the correct solids segregation pattern as well as numerous other flow behaviors characteristic of vertical gas–solid systems, it is now worthwhile to compare model predictions with experimental data. It should be noted, however, that the validity of such comparisons remains in question for a number of reasons. First, as previously discussed, the appropriateness of the constants used in the closure relations of the particle-phase turbulence correlations is uncertain. In addition, the experimental data sets available in the literature may not necessarily represent fully developed flow conditions; if measurements at successive L/D (pipe length/pipe diameter) ratios are shown, the difference between mean variable profiles at different L/D positions can be quite large.

A summary of the experimental systems for which comparisons with model predictions are made is listed in Table 3. This representative set of experimental data is chosen since it contains measurements of different mean variables (local solids velocity, local solids flux, local solids volume fraction, and axial pressure gradient) obtained over a considerable range of system conditions. Comparisons with additional data sets are given in Hrenya (1996). In Figure 12, the model prediction for the solids velocity profile is displayed along with the experimental data of Harris et al. (1993). The overall quantitative match is quite good, although the model does slightly overpredict the experimental values in the range $0.4 < r/R < 0.8$. A comparison of the model prediction for the local solids flux with the measurements of Rhodes et al. (1988) is depicted in Figure 13. Unlike the comparison with the Bader et al. (1988) system shown in Figure 6a, the model prediction here shows considerably more solids downflow

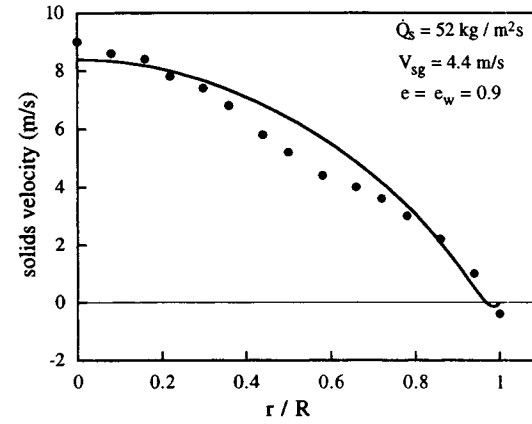

Figure 12. Radial variation of solids velocity predicted by Model 2 vs. experimental data of Harris et al. (1993).

near the pipe wall and more solids upflow in the pipe center than does the experimental data. Note, however, that the data point closest to the wall may not represent the minimum solids flux due to the difficulty in obtaining measurements close to the wall. Figure 14 gives the model prediction for the radial variation of solids volume fraction and the corresponding Weinstein et al. (1986) data. The model prediction is fairly close to the measured values, though the ability of the model in the wall region is again difficult to assess. The final comparison is illustrated in Figure 15, in which the relationship between the required axial pressure gradient and the solids flux for a system at fixed superficial gas velocity is plotted. Although the magnitude of the model predictions compare fairly well with the measurements of Yerushalmi (1986), the predicted slope of the relationship is lower than that demonstrated by the experimental data.

Summary

Previous work has indicated that two mechanical interactions exist that are capable of giving rise to the lateral segregation of solids present in vertical dense-phase flows, namely

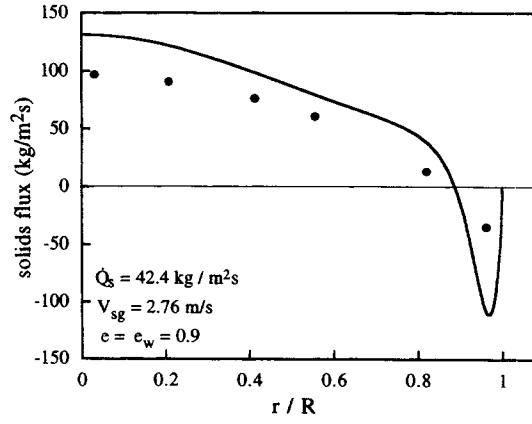

Figure 13. Radial variation of local solids flux predicted by Model 2 vs. experimental data of Rhodes et al. (1988).

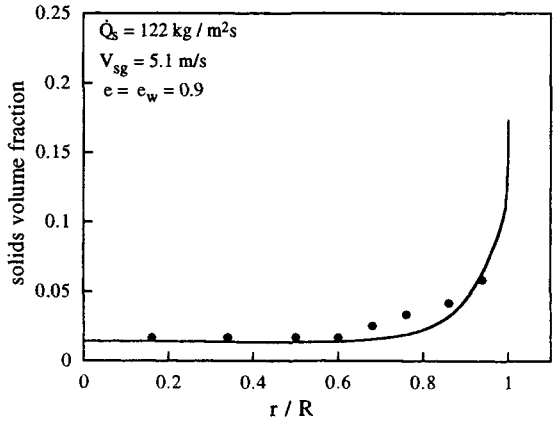

Figure 14. Radial variation of solids volume fraction predicted by Model 2 vs. experimental data of Weinstein et al. (1986).

the interactions among individual particles (Sinclair and Jackson, 1989) and the interactions associated with the collective motion of particles (Dasgupta et al., 1994). In the present work, the combined effect of both mechanisms has been thoroughly investigated. It has been shown that a model (Model 1) that incorporates the effects of both the "laminar" and "turbulent" mechanisms based on the kinetic theory for granular flows and a time-averaging treatment of the governing equations *alone*, respectively, is not adequate. Namely, the extreme sensitivity of the model to inelastic particle–particle collisions cannot be eliminated without adversely affecting other predicted flow features. However, by also considering the effects of particle-phase turbulence on the kinetic theory expressions, it has been shown that the resulting model (Model 2) is able to predict a marked segregation of solids, as well as many of the other flow features characteristic of vertical flows, over a wide range of operating conditions. Perhaps more importantly, though, the model does not manifest an unsatisfactory degree of sensitivity to inelastic particle–particle collisions, a behavior that is common among previous gas–solid flow models based on the kinetic-theory analogy.

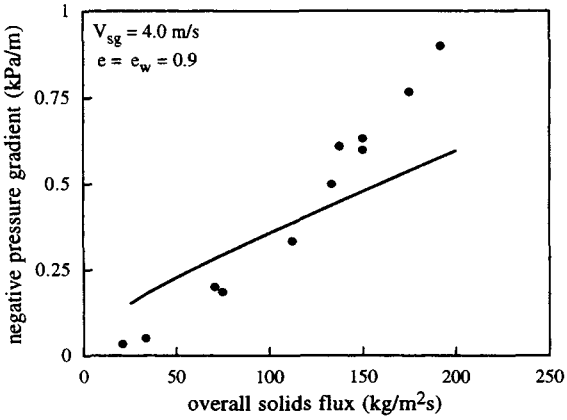

Figure 15. Relation between pressure gradient and overall solids flux predicted by Model 2 vs. the experimental data of Yerushalmi (1986).

It should not be concluded, however, that the model developed herein does not require further modifications. The closures used to describe particle-phase turbulence correlations are somewhat speculative in nature due to the lack of available information about their behavior. Although the physical mechanisms governing particle-phase turbulence are believed to be the same as those governing single-phase turbulence, an exact agreement between the two behaviors is not likely. In addition, the effects of particle-phase turbulence on the kinetic theory expressions for the stress tensor and flux of pseudothermal energy have been ignored in the present formulation. Each of these issues points to the need for an investigation of the effects of turbulent fluctuations in solid-phase variables on the quantities used to describe these flows (e.g., solid-phase stress and pseudothermal energy flux).

Acknowledgments

The authors gratefully acknowledge funding support from the National Science Foundation Presidential Young Investigator Awards Program under grant CTS-9157185 with matching funds from the Dow Chemical Company, the Laboratory Participation Program under Contract DE-AC05-76OR00033 between the U.S. Department of Energy and Oak Ridge Associated Universities, and the Pittsburgh Supercomputer Center.

Notation

g_o = radial distribution function
r = radial coordinate, m
z = axial coordinate, m
δ_{ij} = Kronecker delta
λ_{mfp} = mean free path of particles, m
μ_s = solid-phase laminar viscosity, kg/m s
ν_s = solid-phase laminar kinematic viscosity (= $\mu_s/\rho_s\ \phi_s$), m²/s
θ = azimuthal coordinate, m

Subscript and superscript

r,z,θ = components in cylindrical coordinate system

Literature Cited

Anderson, T. B., and R. Jackson, "A Fluid Mechanical Description of Fluidized Beds," *Ind. Eng. Chem. Fund.*, **6**, 527 (1967).

Bader, R., J. Findlay, and T. M. Knowlton, "Gas/Solids Flow Patterns in a 30.5-cm-Dia. Circulating Fluidized Bed," *Proc. Int. Circulating Fluidized Bed Conf.*, Compiegne, France, p. 123 (1988).

Bolio, E. J., J. A. Yasuna, and J. L. Sinclair, "Dilute Turbulent Gas-Solid Flow in Risers with Particle-Particle Interactions," *AIChE J.*, **41**, 1375 (1995).

Bolio, E. J., and J. L. Sinclair, "Gas Turbulence Modulation in the Pneumatic Conveying of Massive Particles in Vertical Tubes," *Int. J. Multiphase Flow*, **21**, 985 (1995).

Campbell, C. S., and C. E. Brennen, "Computer Simulation of Granular Shear Flows," *J. Fluid Mech.*, **151**, 167 (1985).

Dasgupta, S., R. Jackson, and S. Sundaresan, "Turbulent Gas-Particle Flow in Vertical Risers," *AIChE J.*, **40**, 215 (1994).

Dasgupta, S., R. Jackson, and S. Sundaresan, "Gas-Particle Flow in Vertical Pipes with High Mass Loading of Particles," *Powder Tech.*, in press.

Harris, B. J., J. F. Davidson, and Y. Xue, "Axial and Radial Variation of Flow in Circulating Fluidized Bed Risers," *Proc. Conf. Circulating Fluidized Bed Technology IV*, Hidden Valley, PA, p. 103 (1993).

Hopkins, M. A., and M. Y. Louge, "Inelastic Microstructure in Rapid Granular Flows of Smooth Disks," *Phys. Fluids A*, **3**, 47 (1991).

Hrenya, C. M., "Predicting Dense, Turbulent Gas-Solid Flows in Vertical Risers," PhD Diss., Carnegie Mellon Univ., Pittsburgh (1996).

Johnson, P. C., and R. Jackson, "Frictional-Collisional Constitutive Relations of Granular Materials, with Application to Plane Shearing," *J. Fluid Mech.*, **176**, 67 (1987).
Louge, M. Y., E. Mastorakos, and J. T. Jenkins, "The Role of Particle Collisions in Pneumatic Transport," *J. Fluid Mech.*, **231**, 345 (1991).
Lun, C. K. K., S. B. Savage, D. J. Jeffrey, and N. Chepurniy, "Kinetic Theories for Granular Flow; Inelastic Particles in Couette Flow and Slightly Inelastic Particles in a General Flowfield," *J. Fluid Mech.*, **140**, 223 (1984).
Miller, A., and D. Gidaspow, "Dense, Vertical Gas-Solid Flow in a Pipe," *AIChE J.*, **38**, 1801 (1992).
Myong, H. K., and N. Kasagi, "A New Approach to the Improvement of k-ϵ Turbulence Model for Wall-Bounded Shear Flows," *JSME Int. J.*, **33**, 63 (1990).
Ocone, R., S. Sundaresan, and R. Jackson, "Gas-Particle Flow in a Duct of Arbitrary Inclination with Particle-Particle Interactions," *AIChE J.*, **39**, 1261 (1993).
Patankar, S. V., *Numerical Heat Transfer and Fluid Flow*, Hemisphere, New York (1980).
Pita, J. A., and S. Sundaresan, "Gas-Solid Flow in Vertical Tubes," *AIChE J.*, **37**, 1009 (1991).
Pita, J. A., and S. Sundaresan, "Developing Flow of a Gas-Particle Mixture in a Vertical Riser," *AIChE J.*, **39**, 541 (1993).
Plumpe, J. G., C. Zhu, and S. L. Soo, "Measurement of Fluctuations in Motion of Particles in a Dense Gas-Solid Suspension in Vertical Pipe Flow," *Powder Tech.*, **77**, 209 (1993).
Rhodes, M. J., P. Laussmann, F. Villain, and D. Geldart, "Measurement of Radial and Axial Solids Flux Variations in the Riser of a Circulating Fluidized Bed," *Circulating Fluidized Bed Technology II*, Pergamon Press, Oxford, p. 155 (1988).
Savage, S. B., and M. Sayed, "Stresses Developed by Dry Cohesionless Granular Materials Sheared in an Annular Shear Cell," *J. Fluid Mech.*, **142**, 391 (1984).
Savage, S. B., "Numerical Simulations of Couette Flow of Granular Materials: Spatio-Temporal Coherence and 1/F Noise," *Physics of Granular Media*, D. Bideau and J. Dodds, eds., Nova, Commack, NY, p. 343 (1991).
Sinclair, J. L., and R. Jackson, "Gas-Particle Flow in a Vertical Pipe with Particle-Particle Interactions," *AIChE J.*, **35**, 1473 (1989).
Tsuji, Y., T. Tanaka, and S. Yonemura, "Particle Induced Turbulence," *Appl. Mech. Rev.*, **47**, 75 (1994).
Walton, O. R., H. Kim, and A. D. Rosato, "Microstructure and Stress Differences in Shearing Flows," *Mechanics Computing in 1990's and Beyond*, Vol. 2, H. Adeli and R. L. Sierakowski, eds., ASCE, New York, p. 1249 (1991).
Weinstein, H., M. Shao, and L. Wasserzug, "Radial Solid Density Variation in a Fast Fluidized Bed," *AIChE Symp. Ser.*, 117 (1984). (1984).
Weinstein, H., M. Shao, M. Schnitzlein, and R. A. Graff, "Radial Variation in Void Fraction in a Fast Fluidized Bed," *Fluidization V*, Engineering Foundation, New York (1986).
Wen, C.-Y., and Y. H. Yu, "Mechanics of Fluidization," *Chem. Eng. Progr. Symp. Ser.*, **62**, 100 (1965).
Yerushalmi, J., N. Cankurt, D. Geldart, and B. Liss, "Flow Regimes in Vertical Gas-Solid Contact Systems," *AIChE Symp. Ser.*, **74**, 1 (1978).
Yerushalmi, J., and A. Avidan, "High Velocity Fluidization," *Fluidization*, 2nd ed., J. F. Davidson, R. Clift, and D. Harrison, eds., Academic Press, New York (1985).
Yerushalmi, J., "High Velocity Fluidized Beds," *Gas Fluidization Technology*, D. Geldart, ed., Wiley, New York (1986).

Manuscript received Feb. 25, 1996, and revision received Oct. 22, 1996.